Catalysis Letters, Vol. 117, Nos. 3–4, September 2007 (© 2007)
DOI: 10.1007/s10562-007-9115-8

Photocatalysis of methylene blue on titanium dioxide nanoparticles synthesized by modified sol-hydrothermal process of $TiCl_4$

Sung-Yeon Kim,[a,b] Tae-Ho Lim,[a,b] Tae-Sun Chang,[a,*] and Chae-Ho Shin[b]

[a]*Advanced Chemical Technology Division, Korea Research Institute of Chemical Technology, Daejeon 350-343, Korea*
[b]*Department of Chemical Engineering, Chungbuk National University, Cheongju, Chungbuk 361-763, Korea*

Received 1 April 2007; accepted 2 April 2007

Titanium dioxide nanoparticles were synthesized by the hydrolysis and condensation of $TiCl_4$, an economic titanium precursor, in a mixed solvent of iso-propyl alcohol and water. As-prepared powders were characterized by X-ray diffraction (XRD), Fourier transform infrared spectroscopy (FT-IR), field emission scanning electron microscopy (FE-SEM), energy filtering transmission electron microscopy (EF-TEM). To examine the photocatalytic activity of the as-prepared TiO_2, the photodegradation of MB which is a typical dye resistant to biodegradation has been investigated on TiO_2 powders in aqueous heterogeneous suspensions. The photocatalytic activity of TiO_2 powders prepared by the hydrolysis of $TiCl_4$ in the mixed solutions of iso-PrOH/H_2O exceeded that of commercial TiO_2 powders. The apparent first order rate constants (k_{app}) for the photodegradation of methylene blue (MB) showed a good correlation with the absorbance area obtained by UV-VIS DRS on wavelength in the limits of used lamp emission 300∼420 nm.

KEY WORDS: TiO_2 nanoparticle; photoactivity; methylene blue; $TiCl_4$.

1. Introduction

Nano-sized titanium dioxide (TiO_2) is an excellent candidate for a multi-purpose photocatalyst, because of its optical properties, including a high refractive index leading to a hiding power and whiteness, as well as it chemical stability and relatively low production cost [1]. The photocatalytic approach is attractive in what regard catalytic activity. Titanium dioxide powders, added to organic contaminated water and illuminated by mild UV light, works as a photocatalyst, oxidizing dissolved toxic organic compounds into relatively benign species. Whereas organic compounds are not fully decomposed by conventional technology they can be completely decomposed to H_2O and CO_2 by photocatalysis. In addition, no secondary pollutants are generated in the latter process.

When TiO_2 absorbs a photon of energy greater than or equal to the band gap energy, an electron moves to a conduction band from a valence band. An electron is distributed in the conduction band and an electron vacancy or ''hole'' is distributed in the valence band. If charge separation is maintained, the electron and hole may migrate to the catalyst surface where they participate in redox reactions with adsorbed species. A hole and an electron range respectively at the valence band and conduction band by the irradiation of light. A hydoxyl radical (–OH) and superoxide radical then occur after reacting with water and oxygen in the atmosphere. Therefore, a limiting factor of the photocatalytic reaction is recombination of the electron and hole prior to the superoxide activation step.

With regard to enhancing the catalytic activity and process efficiency of industry, it is important to develop TiO_2 materials with small grain size, high surface area, controlled porosity, and tailor-designed pore size distribution. Moreover, the phase and the degree of crystallinity of the TiO_2 particles also play important roles. For example, numerous studies have confirmed that the anatase phase of TiO_2 is a photocatalytic material for air purification, water disinfection, hazardous waster remediation, and water purification [2,3].

TiO_2 nanoparticles in powder have real advantages in relation to photocatalytic activity. In order to do high activity, several methods of preparation have been reported, such as sol-gel [4,5], hydrothermal [6], and microemulsion methods [7]. Also, powder morphology is affected by the properties of the solvent. Look and Zukoski [8] reported that colloidal stability plays an important role in the development of precipitate morphology. Fang *et al.* [9] used $TiCl_4$ to produce uniform-sized titanium dioxide by using *n*-propanol as a solvent.

In this work, nano-sized titanium dioxide powders are prepared by modified sol-thermal hydrolysis of $TiCl_4$ in the iso-PrOH/H_2O mixed solutions. Titanium dioxide with different crystal structures, particle sizes, formation and morphologies are obtained by simply varying the calcination temperature. To examine the photocatalytic

*To whom correspondence should be addressed.
E-mails: tschang@krict.re.kr; chshin@chungbuk.ac.kr

activity of the as-prepared TiO_2, the photodegradation of methylene blue (MB) which is a typical dye resistant for water purification has been investigated. The photocatalytic activity of the prepared titanium dioxide nanoparticles was higher than that of typical commercial nanosized-TiO_2 (Ishihara ST-01, ST-21) under same operating conditions. Also, the photoactivity of MB showed a good correlation with the absorbance area obtained by UV-VIS DRS.

2. Experimental

2.1. Preparation of nano-sized titanium dioxide powders

The preparation of nano-sized titanium dioxide was carried out using a sol-hydrothermal method of titanium tetrachloride (Extra pure grade, $TiCl_4$, Yakuri Pure Chemicals Co., Japan), which was used as a starting material without any further purification. $TiCl_4$ was dissolved in deionized water maintaining at 4 °C to avoid rapid precipitation. The concentration of titanium was adjusted to 1.0, 2.0–3.0 M. The aqueous solution was mixed with mixed solvent of iso-propyl alcohol and water with a volume ratio of 2. Hydroxypropyl cellulose (HPC) (75–150 cps, molecular weight ~100,000, Aldrich) with a concentration 6.4×10^{-4} g/cm^3 was added to the solution as a steric dispersant. The aqueous solution was vigorously stirred for 4 h at room temperature. The solution was then heated and aged at 70 °C for 1 h to carry out hydrothermal hydrolysis and then white precipitate was formed. After precipitation, the solution was neutralized with a 2% NH_4OH solution adding dropwise in order to remove chloride ions. The precipitate was separated by filtration and washing three times with deionized water, and finally rinsed with acetone. The obtained precipitate was aged in an autoclave at 250 °C for 4 h (SY-250). After aging the samples were calcined at 400 °C (SY-400) and 600 °C (SY-600) for 2 h under flowing air, respectively. We called the prepared samples that it is SY-x-y (x: Ti concentration, y: calcinations temperature) here.

2.2. Characterization

Powder X-ray diffraction (XRD) patterns were collected on a D/MAX-IIIB diffractometer with CuK_α radiation at 40 kV and 40 mA. XRD was used for crystal phase, estimation of the anatase-to-rutile ratio and the particle size of each phase present [10]: $X = 1/1 + 0.8(I_A/I_R)$, where X is the fraction of rutile phase; IA the integrated (101) intensity of anatase; IR is the integrated (110) intensity of rutile. The crystallite sizes were determined from the broadening of corresponding X-ray spectral peaks by the Scherrer formula using the peak of the anatase (101) at $2\theta = 25.35°$ and the rutile (110) at 27.45°: $L = K\lambda/(\beta\cos\theta)$, Where L is the particle size, λ is the wavelength of the X-ray radiation ($CuK\alpha = 0.15418$), K is usually taken as 0.89, and β is the line width at half-maximum height, after subtraction of equipment broadening.

A microstructural investigation of the fracture surface of the compacted samples was conducted on Jeol JSM-6700F field emission scanning electron microscope (FE-SEM) and Carl Zeiss EM 912 Omega energy filtering transmission electron microscope (EF-TEM). The samples were dispersed in absolute ethanol and sonicated ultrasonically to separate out individual particles for the determination of particle size.

Jasco 610 Fourier-transform infrared spectrophotometer (FT-IR) was used to characterize the functional groups of the particles. FT-IR measurements were carried out in the region from 400 to 4000 cm^{-1}. The sample was ground with dried potassium bromide (KBr) powder, and compressed into a disc. The KBr disc was subjected to analysis by an IR spectrophotometer.

Shimadzu UV-2401PC UV/VIS spectrophotometer was used for the determination of dye disappearance kinetics, recording the spectra over 200–600 nm. A calibration plot based on Beer-Lambert's law was established, relating the absorbance to the concentration. The plot was determined at the maximum of absorbance of MB.

BET surface area and total pore volume were measured on a Micromeritics ASAP 2010 nitrogen adsorption apparatus.

2.3. Photodegradation of MB

In order to examine the photocatalytic activity of TiO_2 prepared, the photodegradation of MB blue has been investigated in aqueous heterogeneous suspensions equipped with UV radiation source. A biannular quartz glass reactor with the lamp immersed in the inner part was used for all photocatalytic experiments. In a MB aqueous solution of 1,000 mL with a concentration of 0.05 mM of MB, sample powders of 0.3 g were dispersed under ultrasonic vibration for 5 min. A 9 W black light blue lamp (Philips, PLS9W/08.BLB) was used as the UV radiation source. All experiments were conducted at room temperature without a supply of air.

The samples were centrifuged to separate the TiO_2 from the solution, and the absorption was measured at 665 nm of the remained solution [11,12]. The absorption was converted to relative concentration of MB (C/C_0) referring to a standard curve and displayed linear behavior between relative concentration and the absorption at this wavelength.

For comparison the photocatalysis of MB on commercial TiO_2 powders which are from Ishihara (ST-01, ST-21) were conducted under same operating conditions.

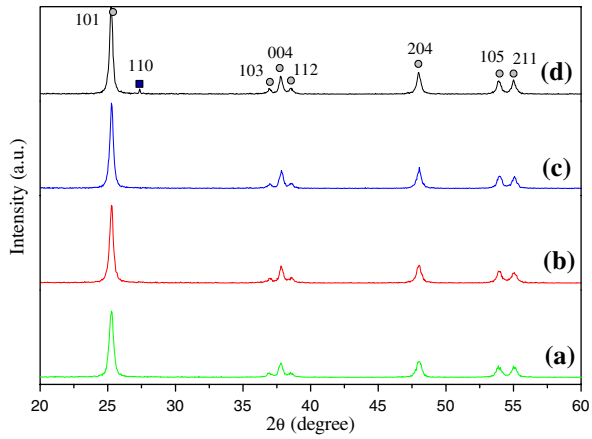

Figure 1. Powder XRD patterns of the samples (SY-2-y) as-prepared from $TiCl_4$ solution aged at 250 °C for 4 h (a), calcined at 400 °C (b), 500 °C (c) and 600 °C (d) for 2 h under flowing air.

3. Results and discussion

Figure 1 shows the effect of calcination temperature on the crystallinity of the TiO_2 prepared (SY-2-y) with iso-PrOH/H_2O solvent. Figures 1 (a)∼(c) show TiO_2 prepared were notably formed to anatase structure (JCPDS 21–1272). When TiO_2 powders are calcined at higher temperatures least above 450 °C, the transformation of TiO_2 anatase to rutile may occur [13]. However, TiO_2 prepared with iso-PrOH/H_2O solvent after calcination at 600 °C consists of maximum 3% quantity of rutile (figure 1(d)). BET surface areas of SY photocatalysts are significantly declined with increasing calcination temperature as given in table 1.

The particle size was estimated by the Scherrer formula [14], which is generally accepted to estimate the mean particle size [15]. Sunstrom *et al.* [16] reported a similar XRD pattern for TiO_2 prepared by the hydrodynamic cavitation method. The particle size calculations were found to be around 5–17 nm.

The particle size of the powder as function of calcination temperature and concentration of Ti is shown in table 1. Gradually, the particle size increases with increasing calcination temperature and concentration of Ti. The growth of particle becomes slowly at low calcination temperatures, but it is rapidly at high calcination temperatures. Hence, the particle size increases very quickly with the increasing of calcination temperature.

Figure 2 shows the SEM and TEM image of a sample (SY-2-400) aged in an autoclave at 250 °C for 2 h and subsequently calcined at 400 °C for 2 h. The particle size and morphology are almost uniform, as shown in figure 2. Uniform and ultrafine TiO_2 nanoparticles were observed in SY-400 and this crystallite size was in good agreement with the calculated value from the broadening of XRD peaks.

Hydroxypropyl cellulose (HPC) was used as a steric dispersant. HPC has been known to provide steric stabilization during the precipitation of TiO_2 from an alcohol solution. K. D. Kim and H. T. Kim [17] reported that HPC adsorbed onto the particles prevents agglomeration during growth. The excess HPC would be a nucleation site for precipitation. As the concentration of HPC increase, the particle size and the size distribution would decrease. That is to say, there is an optimum concentration of dispersant. The concentration of HPC at 0.35×10^{-3} g/cm^3 yielded the best spherical titania particles.

The results of FT-IR spectra are summarized in figure 3 as a function of calcination temperature. The number of hydroxyl groups on the surface of TiO_2 is proportional to the intensity of the peak at 3420 cm^{-1}. It is found that as the substrate surface area is increased, the hydroxyl groups on the surface also

Table 1
Surface and structural properties of commercial TiO_2 and prepared SY-x-y series (SY-x-y, x: Ti concentration, y: temperature)

Sample	Particle size[a] (nm)	BET surface area[b] (m^2/g)	Phase[c]	Integral of spectrum[d] (nm)	k_{app}[e] $\times 10^{-3}$ (min^{-1})
ST-01	7	321	Anatase (100%)	83.6	1.2815
ST-21	20	70	Anatase (100%)	80.7	0.9143
SY-1-250	6	109	Anatase (100%)	79.8	0.8758
SY-1-400	8	90	Anatase (100%)	86.8	1.3487
SY-1-600	10	79	Anatase (100%)	83.5	1.2383
SY-2-250	5	113	Anatase (100%)	81.6	0.9614
SY-2-400	8	98	Anatase (100%)	90.2	1.5128
SY-2-600	17	46	Anatase (97%) + Rutile (3%)	71.5	0.6602
SY-3-250	12	85	Anatase (100%)	70.2	0.6237
SY-3-400	18	59	Anatase (95%) + Rutile (5%)	81.5	0.9395
SY-3-600	25	36	Anatase (85%) + Rutile (15%)	69.3	0.5124

[a]Obtained by Scherrer equation.
[b]BET surface area calculated from the linear part of the BET plot (P/P_0 = 0.1595–1994).
[c]Characterized by XRD.
[d]Obtained by UV-VIS DRS on wavelength in the limits of used lamp emission 300∼420 nm.
[e]The apparent first order rate constants calculated by MB photocatalysis.

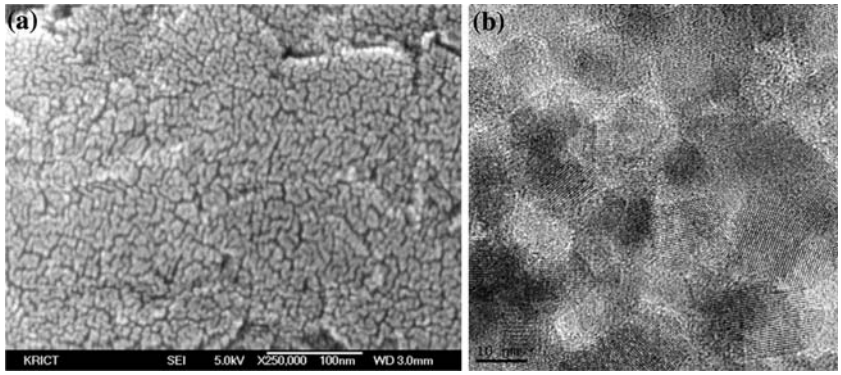

Figure 2. FE-SEM (a) and EF-TEM (b) images for the TiO_2 powders (SY-2-400) prepared by sol-hydrothermal method.

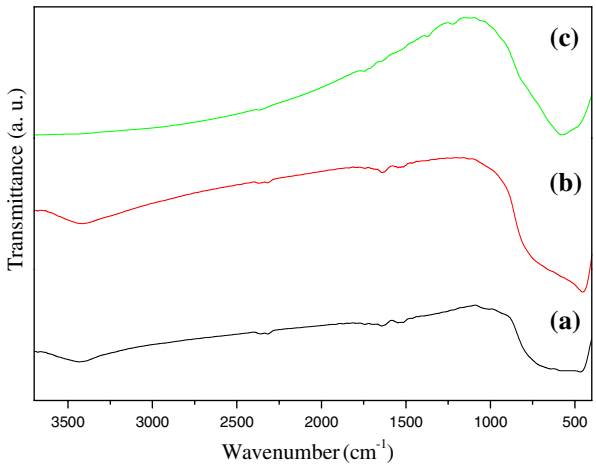

Figure 3. Fourier transform IR spectra of the samples (SY-2-y) as-prepared from $TiCl_4$ solution aged in 250 °C for 4 h (a), calcined at 400 °C (b) and at 600 °C (c) for 2 h under flowing air.

become larger. The peak at 1643 cm^{-1} is due to the bending vibration of water molecules suggesting the presence of water which corresponds to the surface adsorbed water and hydroxyl groups [18]. We predicted that SY-2-600 would have much fewer surface OH groups than SY-2-250 and SY-2-400 because the calcination at high temperature (600 °C) diminishes the surface OH groups of nano-sized titanium dioxide particles. Hydroxyl groups are adsorption sites for compounds tending to form hydrogen bond. Such compounds are usually water-soluble. On the contrary, water-insoluble compounds would tend to adsorb on hydrophobic adsorption sites. Hydroxyl groups are progressively removed in the thermal treatment of TiO_2. The loss of surface hydroxyl groups causes a decrease in the photoactivity of nanoparticles because the photocatalysis is basically a surface phenomenon and is very sensitive to the kind of chemical species that is attached on the surface of TiO_2 nanoparticles. Larbot *et al.* [19] and Chhor *et al.* [20] observed the same bands, which they assigned to $v_{Ti\text{-}O} = 653\text{–}550 cm^{-1}$ and $v_{Ti\text{-}O\text{-}Ti} = 495\text{–}436\ cm^{-1}$.

The nitrogen adsorption-desorption isotherm of material obtained under different conditions indicates a mesoporous structure, as seen in figure 4. The isotherm is of type IV, characteristic of mesoporous material [21]. The hysteresis loop observed with the isotherm was mainly type H1, which is characterized by agglomerates of approximately uniform size, giving rise to a narrow pore size distribution. The sharp decline in the desorption curve is indicative of mesoporosity. The pore size distribution calculated from the desorption branch of the nitrogen isotherm by the BJH method reveals an average pore size of 9.8 (SY-2-250), 11.6 nm (SY-2-400) and 13.8 nm (SY-2-600). The pore size is in the range of 6–11 nm, 7–12 nm and 8–14 nm respectively. To confirm the increase in crystallinity as temperature increases, specific surface area measurements were carried out. As anticipated, we found that higher calcination temperature yielded lower specific surface area. Table 1 indicates that commercial TiO_2 and samples prepared by our method have mesoporous structures. These structures are the result of the formation of pores between TiO_2 nanoparticles [22,23].

Figure 5 depicts UV-VIS diffuse reflectance spectra (UV-VIS DRS) of SY-2-y catalysts compare with commercial photocatalysts. These spectra are noticeably different in the ultraviolet area. Absorbance area of a sample can be expressed quantitatively as an integral of diffuse reflectance spectrum on wavelength in the limits of used lamp emission 300 $\sim$ 420 nm.

This characteristic obtained by UV-VIS DRS spectroscopy is represented in table 1. One can see that the absorbance area in the ultraviolet region grows with rise of calcinations temperature for samples aged at 250 °C, calcined at 400 °C and then diminishes for the sample calcined at 600 °C. Samples calcined at 400 $\sim$ 600 °C differ with the absorbance are according to the concentration of Ti. Specific surface area of the SY-photocatalysts steadily decreases with the increase in temperature of thermal treatment. This is obviously due to progressive aggregation of small crystallites into larger particles. In spite of the fact that the specific surface area diminishes, absorbance area increases until

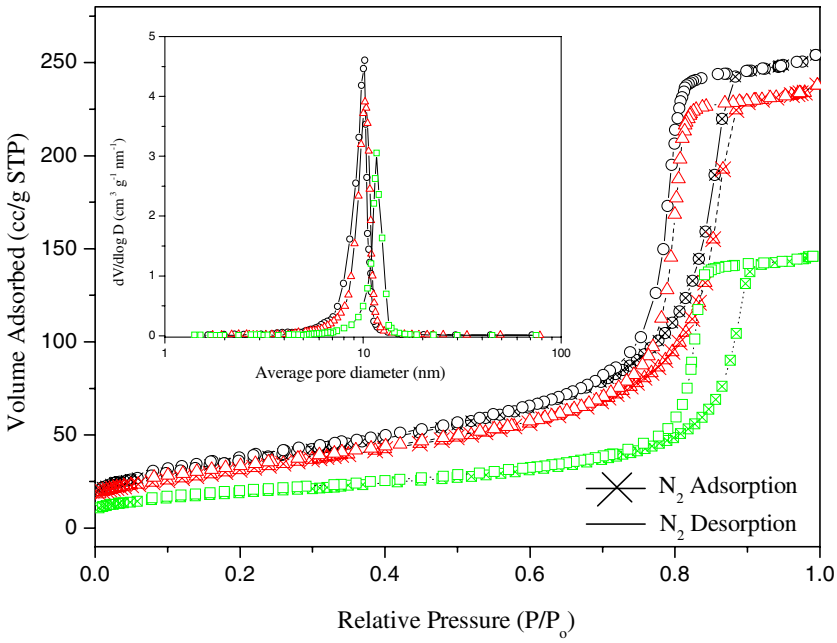

Figure 4. The nitrogen adsorption-desorption isotherms of mesoporous titanium dioxide (a) and BJH pore size distribution (b) for the samples (SY-2-y) as-prepared from $TiCl_4$ solution aged in 250 °C for 4 h (○), calcined at 400 °C, (△) and at 600 °C (□) for 2 h under flowing air.

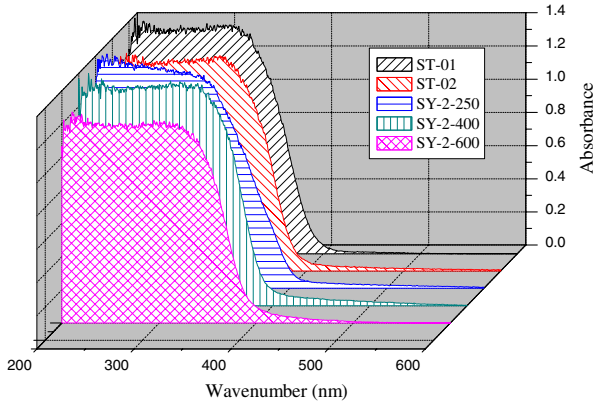

Figure 5. Comparison of UV/VIS DRS spectra for SY-2-y TiO_2 as-prepared and commercial TiO_2 photocatalysts.

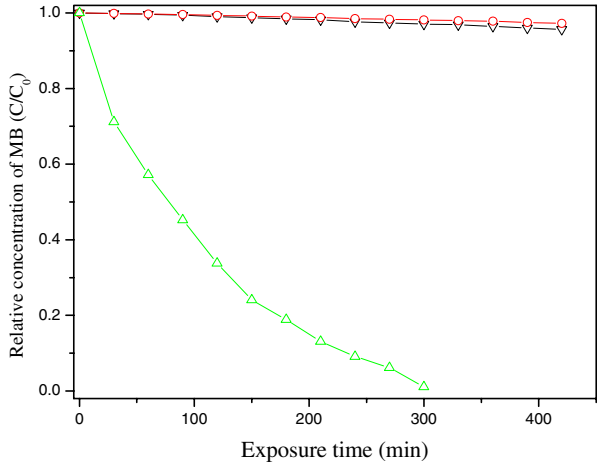

Figure 6. Photodegration of MB solution in UV irradiated TiO_2 (SY-2-400, △), direct UV without TiO_2 (○), and the dark with TiO_2(▽).

the temperature attains 400 °C and decreases only then. Absorbance area (integral of UV spectrum) is fairly related with photocatalytic activity [24]. It is inclined to use absorbance area rather than reaction rate per unit of surface area as characteristic of photocatalytic activity because it is very difficult to determine the surface area that actually takes part in the reaction. Absorbance area was ranked in order from the highest to the lowest: SY-2-400 > SY-1-400 > ST-01 > SY-1-600 > SY-2-250 > SY-3-400 > ST-21 > SY-1-250 > SY-2-600 > SY-3-250 > SY-3-600.

Most of our experiments were run at an initial MB concentration of 0.05 mM, at which adequate color changes (hypsochromic effect) of the TiO_2 particle surface resulting from photocatalytic degradation of MB were observed. The peaks between 600 and 700 nm were assigned as the absorption of the conjugated π-system [25]. MB degradation was also observed in the dark condition with direct UV photolysis without TiO_2 (figure 6). The result showed that MB was hardly decomposed without TiO_2 and UV light irradiation. The difference in the photoactivity of SY-250, SY-400 and SY-600 is attributed to calcination. In figure 7, relative concentration C/C_0 of MB in solution is plotted in logarithmic scale against irradiation time of UV rays for shown on the prepared TiO_2 and commercial TiO_2. There are two major variables that can vary during calcination. The positive change predicted is an increase of crystallinity and the negative change is a reduction of surface OH groups. The loss

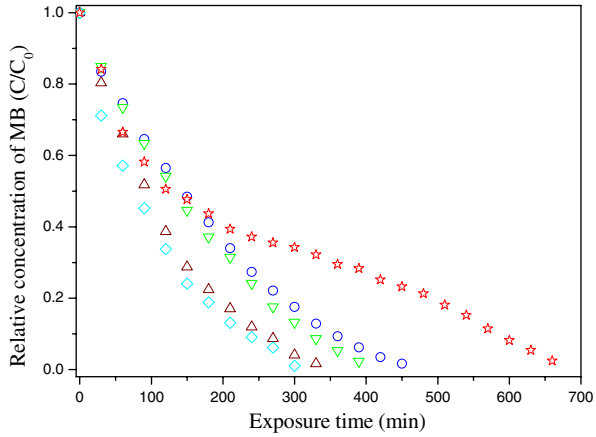

Figure 7. Photodegradation of MB solution in the prepared TiO_2 and commercial photocatalysts; ST-01 (△), ST-02 (O), SY-2-250 (▽), SY-2-400 (◇), SY-2-600 (☆).

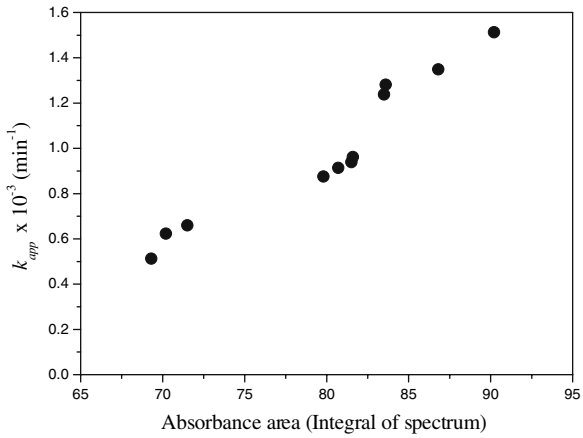

Figure 8. Correlation between the absorbance area of UV region and the apparent first order rate constants (k_{app}) for the prepared TiO_2 and commercial photocatalysts with anatase phase.

of surface OH groups causes a decrease in the photoactivity of nanoparticles because the photocatalysis is basically a surface phenomenon and is very sensitive to the kind of chemical species that is attached on the surface of the titanium dioxide particles. SY-400 is superior to SY-250 and SY-600 in term of photocatalytic activity.

Excessive quantities of hydroxyl groups on the TiO_2 surface have detrimental effect on photocatalytic oxidation, but small quantities are essential for sustained reation rate [26]. Therefore, the peak in photocatalytic activity at treated temperature 400 could be attributed to optimal quantity of hydroxyl groups on the TiO_2 surface. However, the decrease in specific surface area and growth of crystallinity should not be disregared because these factors are also important for photocatalytic activity [27].

As a comparison, MB degradation over TiO_2 (ST-01, ST-21) was also observed with the same method. The plots of figure 7 provide a comparison between SY-2-y and commercial photocatalysts. On the basis of the results, Photocatalytic activity was ranked in order from the highest to the lowest: SY-2-400 > SY-1-400 > ST-01 > SY-1-600 > SY-2-250 > SY-3-400 > ST-21 > SY-1-250 > SY-2-600 > SY-3-250 > SY-3-600.

At present, although the detailed pathway of MB degradation reaction are not yet clear this study demonstrated that MB could be degraded largely over the SY photocatalysts under UV light irradiation.

In analyzing the kinetic data of photocatalyzed oxidations, mediated by photo-activated semiconductor particles, the data were fitted to the simple rate expression of the Langmuir-Hinshelwood (L-H) form as follows (equation (3)):

$$R = -\frac{dC}{dt} = \frac{K_{Ad}kC_0}{1 + K_{Ad}C_0} \tag{3}$$

where C_0, K_{Ad} and k are the initial concentration of MB, the adsorption coefficient and the reaction rate constant respectively. The integration of equation (3) yields equation (4) as follows:

$$t = \frac{1}{K_{Ad}k} In\left(\frac{C_0}{C}\right) + \frac{1}{k}(C_0 - C) \tag{4}$$

The integrated form of equation (3) for a low initial concentration of MB of this study can be written as follows (equation (5)):

$$In\left(\frac{C}{C_0}\right) = -K_{Ad}kt = -k_{app}t \tag{5}$$

where k_{app} is the apparent reaction rate constant and t is the reaction time.

Rate constant k_{app} has been chosen as the basic kinetic parameter for different systems, since it is independent of used concentration [28,29].

The apparent first order rate constants (k_{app}) for the prepared photocatalysts are shown in table 1. As shown in figure 8, there is respectively a similar result to table 1 in the absorbance area and the apparent first order rate constant.

4. Conclusions

TiO_2 particles with small grain size, high surface area, and OH surface groups play an important role in catalytic activity and process efficiency. Titanium dioxide nanoparticles were prepared by hydrolysis using $TiCl_4$, an economic titanium precursor, in a mixed solvent of iso-proanol and water. The prepared titanium dioxide exists in the form of nanocrystalline anatase with higher specific surface area, OH surface groups and absorbance area. Specially, the absorbance area was directly proportional to photoactivity. This correlation is used for quick estimation of photoactivity without real photocatalytic measurements.

The photocatalytic degradation of MB was examined by UV-illuminated aqueous TiO_2 dispersions, a

representative of polluting dyestuff in textile effluents. The photocatalytic activities were ultimately evaluated by the rate constant k for MB decomposition reaction, which was determined from the linear relation between the logarithm of relative concentration of MB in solution $\ln(C/C_0)$ and irradiation time. The photocatalytic activity was ranked from highest to lowest: SY-2-400 > SY-1-400 > Ishihara ST-01 > SY-1-600 > SY-2-250 > SY-3-400 > Ishihara ST-21 > SY-1-250 > SY-2-600 > SY-3-250 > SY-3-600.

References

[1] T. Sugimoto, X. Zhou and A. Muramatsu, J. Colloid Interface Sci. 259 (2003) 43.
[2] Rajeev K. Wahi, William W. Yu and Ynping. Liu, J. Mol. Catal. A: Chem. 242 (2005) 48.
[3] A. Fujishima, T.N. RaO and D.A. Tryk, J. Photochem. Photobiol. C 1 (2000) 1.
[4] G. Colon, M.C. Hidalgo and J.A. Navio, Catal. Today 76 (2002) 91.
[5] M. Keshmiri, M. Mohseni and T. Troczynski, Appl. Catal. B: Env. 53 (2004) 209.
[6] M. Inagaki, Y. Nakazawa, M. Hirano and Y.M. Toyoda, Int. J. Inorg. Mater. 3 (2001) 809.
[7] S.S. Hong, M.S. Lee, H.S. Hwang, K.T. Lim, S.S. Park, C.S. Ju and G.D. Lee, Solar Energy Mat. Solar Cells 80 (2003) 273.
[8] J.L. Look and C.F. Zukoski, J. Am. Ceram. Soc. 75 (1992) 1587.
[9] C.S. Fang and Y.W. Chen, Mater. Chem. Phys. 78 (2003) 739.
[10] R.A. Spurr and H. Myers, Anal. Chem. 24 (1957) 760.
[11] J. Tang, Z. Zou, J. Yin and J. Ye, Chem. Phys. Lett. 382 (2003) 175.
[12] F.B. Li and X.Z. Li, Appl. Catal. A 228 (2002) 15.
[13] C. Byun, J.W. Jang, I.T. Kim, K.S. Hong and B.W. Lee, Mater. Res. Bull 32 (1997) 431.
[14] B.R. Sankapal, M.Ch. Lux-Steiner and A. Ennaoui, Appl. Surf. Sci. 239 (2005) 165.
[15] S.J. Kim, S.D. Park, Y.H. Jeong and S. Park, J. Am. Ceram. Soc. 82 (1999) 927.
[16] J.E. Sunstrom IV, W.R. Moser and B. Marshik-Guerts, Chem. Mater. 8 (1996) 2061.
[17] K.D. Kim and H.T. Kim, Powder Technol. 119 (2001) 164.
[18] Z. Ding, G.Q. Lu and P.F. Greenfield, J. Phys. Chem. B 104 (2000) 4815.
[19] A. Larbot, J. Marignan and J.F. Quinson, J. Non-Crystall. Solids 147–148 (1992) 157.
[20] K. Chhor, J.F. Bocquet and C. Pommier, Mater. Chem. Phys. 32 (1992) 249.
[21] Y. Zhang, H. Zhang, Y. Xu and Y. Wang, J. Solid State Chem. 177 (2004) 3490.
[22] J.C. Yu, J.G. Yu, L.Z. Zhang and W.K. Ho, J. Photochem. Photobiol. A 148 (2002) 263.
[23] W. Hung, X. Tang, Y. Wang, Y. Koltypin and A. Gedanken, Chem. Commun. 15 (2000) 1415.
[24] A.V. Vorontsov, A.A. Altynnikov, E.N. Savinov and E.N. Kurkin, J. Photochem. Photobiol. A Chem. 144 (2001) 193.
[25] P. Qu, J. Zhao, T. Shen, H. Hidaka and N. Serpone, Environ. Sci. Technol. 33 (1999) 2081.
[26] L. Cao, A. Huang, F.J. Spiess and S.L. Suib, J. Catal. 188 (1999) 48.
[27] Z. Zhang, C.C. Wang, R. Zakaria and J.Y. Ying, J. Phys. Chem. B 102 (1998) 10871.
[28] J. Matos, J. Laine and J.M. Herrmann, Appl. Catal. B 18 (1998) 281.
[29] S. Qourzal, A. Assabbane and Y. Aic-Ichou, J. Photochem. Photobiol. A Chem. 163 (2004) 317.